bioresources.com

Contributions of Basic Chemical Components to the Mechanical Behavior of Wood Fiber Cell Walls as Evaluated by Nanoindentation

Xinzhou Wang,[a,b] Yanjun Li,[c,d,e] Yuhe Deng,[a,*] Wangwang Yu,[a,f] Xuqin Xie,[d] and Siqun Wang,[b,e,*]

Selective chemical extraction was applied to gradually remove classes of chemical components from wood cell walls. Nanoindentation was performed on the control and treated wood cell walls to evaluate the contributions of the chemical components to the cell walls by measuring the elastic modulus, hardness, and creep compliance. Burger's model was applied to simulate the process of nanoindentation and to gain insight into the response of visco-elastic properties to the chemical components. Wood extractives showed limited effects on the cell-wall mechanics; however, the removal of hemicelluloses and lignin resulted in reductions of 11.7% and 28.4%, respectively, in the elastic modulus and 14.8% and 30.4%, respectively, in the hardness. The extraction of hemicelluloses and lignin reduced the resistance of wood cell walls to creep. Furthermore, the extracted parameters from Burger's modeling indicated that cellulose exhibited the greatest influence on the mechanical properties of wood cell wall, while hemicelluloses exhibited the greatest contribution to cell-wall viscosity, and lignin contributed extensively to cell-wall elasticity.

Keywords: Cell wall; Chemical component; Mechanical behavior; Nanoindentation

Contact information: a: College of Materials Science and Engineering, Nanjing Forestry University, Nanjing 210037, P.R. China; b: Center for Renewable Carbon, University of Tennessee, Knoxville, TN 37996, USA; c: School of Engineering, Zhejiang Agriculture and Forestry University, Linan, P.R. China; d: Dehua Tubao New Decoration Material Co., Ltd., Zhejiang 313200, P.R. China; e: Key Laboratory of Wood Science and Technology in Zhejiang Province; f: School of Mechanical Engineering, Nanjing Institute of Industry Technology, Nanjing 210023, P.R. China;
* Corresponding author: dengyuhe@hotmail.com; swang@utk.edu

INTRODUCTION

Wood has been widely used for the construction of homes and structures because of its good machinability, beautiful appearance, and excellent mechanical properties in view of a low density. Wood fibers also can be considered environmentally friendly alternatives for use as reinforcement in engineering polymeric materials (Askanian *et al*. 2015). However, wood also possesses some intrinsic features, such as visco-elasticity, that restrict its application in large structures that require long-term loading. Wood is an anisotropic composite material, which consists of numerous cells that are oriented in the axial and radial directions. The wood cell wall is composed of layers of varying thickness, and the chemical composition dominates the natural properties of wood. Thus, knowledge about the specific molecular mechanical phenomena at the cellular and subcellular levels is of great importance for understanding the mechanical behavior of wood materials used for large-scale applications and the optimization of the design of wood-based composites.

Wood cell walls are composed of microfibrils of cellulose, hemicelluloses, and lignin. In recent decades, the individual structural and chemical properties of cell-wall constituents have been extensively investigated (Nishino *et al*. 2004; Abraham *et al*. 2011). Furthermore, techniques that directly sense responses of whole wood on a molecular level, such as thermal and dynamic mechanical analyses, have been applied to accurately assess the effect of wood components on the cell wall's mechanical behavior (Placet *et al*. 2007; Zelinka *et al*. 2012). Consequently, most of the research targeted the dynamic mechanical performance of isolated wood components (cellulose or lignin) or focused on the whole wood.

The contributions made by individual wood polymers, as well as their interactions, to the composite's properties as a whole, has not been evaluated qualitatively. Furthermore, there is limited research pertaining to how the main components of wood affect the static mechanical properties of wood cell walls at the submicron-scale.

To obtain a better understanding of the relationships between the chemical components and the mechanical behavior at the cell-wall level, new methodological approaches, such as *in-situ* experiments, are required. Nanoindentation has been well recognized as a technique that facilitates the measurement of properties at the micrometer- or nanometer-scale (Oliver and Pharr 1992). Recent developments in these measurement techniques have further extended the usefulness of indentation tests at the cell-wall level of biological tissues (Wimmer *et al*. 1997). During the past decade, a large number of useful engineering properties of biomaterials, including wood (Yu *et al*. 2011; Meng *et al*. 2013; Wang *et al*. 2014), bamboo (Li *et al*. 2015), crop stalks (Wang *et al*. 2013), and others, have been identified by means of nanoindentation.

In the present study, the hemicellulose and lignin contents were removed from wood cell walls gradually, and then the chemical structure, cellulose crystallinity, and microstructure of the treated wood cell walls were analyzed by Fourier transform infrared spectroscopy (FTIR), X-ray diffraction (XRD), and scanning electron microscopy (SEM). The mechanical properties, including the elastic modulus, hardness, and creep compliance of control and treated wood cell walls were measured using nanoindentation. The visco-elastic properties of wood cell walls and their interrelation with the chemical components were investigated based on Burger's model.

EXPERIMENTAL

Materials

The wood species chosen was *Salix discolor*, a hardwood, which was collected from a traditional plantation located in Jiangsu Province, China. Several small wood blocks, with the dimensions of approximately $2 \times 2 \times 10$ mm^3 (tangential $\times$ radial $\times$ longitudinal), were obtained from the bottom of the tree trunk at the same growth ring to avoid artefacts resulting from natural heterogeneity. The chemicals including toluene, ethanol, sodium hydroxide, sulphuric acid, nitric acid, acetic acid, sodium chlorite, *etc*. (Jiuyi Chemicals, Inc., Shanghai, China.), were used to extract the compounds of wood. All reagents used were of analytical grade.

Method

Chemical extraction

Step I: Benzene-ethanol extraction

　　　The wood blocks were randomly assigned for different chemical treatments. As shown in Fig. 1, a portion of the samples were untreated (sample A, the control), and the remaining samples were first extracted with toluene/ethanol (2:1, v/v) in a Soxhlet apparatus for 6 h. Samples that were free of extractives (sample B) were then filtered, washed with acetone, and oven-dried at 60 ℃ until a constant weight was obtained. The measurement accuracy of the constant weight was 0.001 g.

Step II: Hemicellulose removal

　　　Sample B underwent a successive extraction of hemicellulose by treatment with 6.0%, 8.0%, and 10.0% NaOH at 60 °C for 2 h (Nelson 1961). The obtained sample (sample C) was then washed with acetone and dried in a vacuum oven at 60 °C until a constant weight was achieved.

Step III: Delignification

　　　Sample C was delignified using an aqueous solution of 0.3% $NaClO_2$ buffered with acetic acid at pH 4.9 for 4 h at 80 °C (Kataoka and Kondo 1998). Fresh doses of sodium chlorite and acetic acid were added at hourly intervals without the withdrawal of any liquor. The initial liquor-to-wood ratio was 13:1. Finally, the obtained sample (sample D) was washed and dried.
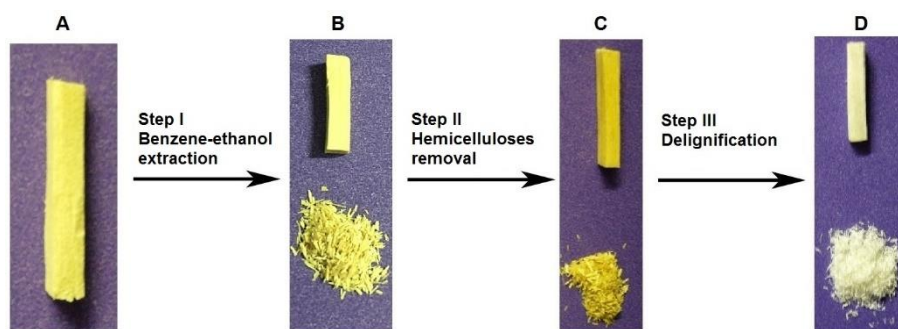

Fig. 1. Photographs indicating the preparation of wood samples for measurements: sample A (control), sample B (benzene-ethanol extracted), sample C (alkaline treated), and sample D (delignified)

Chemical component measurement

　　　The control wood and treated wood were ground in a mill to a homogeneous flour for chemical component analysis, as shown in Fig. 1. The solvent extractives were determined according to the GB/T 2677.6 (1994) standard method, and holocellulose was determined according to Wises's sodium chlorite method (Wise *et al*. 1946). Cellulose was measured using the Kurschner-Hoffner's nitric acid method (Browning 1967), and the lignin content was determined by the acid-insoluble Klason lignin method (hydrolysis with 72% H_2SO_4), according to the GB/T 2677.8 (1994) standard method. The hemicellulose content was calculated by subtracting the cellulose content from the holocellulose content. The relative amount of the chemical components (*X*) of the control and treated woods were estimated according to the following equation,

$$X\ (\%)\ =\ \frac{m_x}{m_o} \times 100 \tag{1}$$

where m_0 is the initial mass of each sample (g) and m_x is the mass of the solvent extractives (g), *i.e*., holocellulose, cellulose, and lignin.

FTIR analysis

Fourier transform infrared spectroscopy measurements were performed on both the control and treated wood to evaluate the hemicellulose extraction and the degree of delignification of the wood cell walls. Samples were first ground and screened into flour of sizes between 40 and 60 mesh. All spectra were collected in the range 4000 to 400 cm^{-1}, with a resolution of 4 cm^{-1}, using a PerkinElmer FTIR spectrometer (Perkin Elmer spectrum one, Waltham, MA, USA).

X-ray diffraction analysis

Crystalline structures of the samples were analyzed by wide-angle X-ray diffraction on a Rigaku Uitima IV instrument (Tokyo, Japan). X-ray diffraction measurements were equipped with a Cu Kα radiation (λ= 0.154 nm), operating at 40 kV and 30 mA. The XRD pattern was recorded within an angle range of 2θ from 5° to 45°, with a scanning rate of 0.05°·s^{-1}. The relative degree of crystallinity (C_rI, %) was calculated according to Segal *et al*. (1959),

$$C_rI\ (\%)\ =\ \frac{I_{002} - I_{am}}{I_{002}} \times 100 \tag{2}$$

where I_{002} represents the intensity of the peak corresponding to the plane in the sample with the Miller indices 002 at a 2θ angle of between 22 to 24 degrees (a.u.) and I_{am} represents only the intensity of diffraction of the amorphous part of the diffractogram (a.u.).

Nanoindentation measurement

Wood samples were cut into smaller blocks of $2 \times 2 \times 5$ mm^3 (T × R × L). According to the method in Meng *et al*. (2013), the samples were tested without embedded epoxy resin to avoid resin penetration. Each sample was mounted on a metal holder designed for ultramicrotomy to obtain a smooth surface with a diamond knife.

As shown in Fig. 2a, nanoindentation was performed on a Hysitron TriboIndenter system (Hysitron Inc., Eden Prairie, MN), equipped with scanning probe microscopy (SPM) and a Berkovich indenter, at room temperature (20 °C) and a relative humidity of $45 \pm 2\%$. All samples were maintained in the TriboIndenter chamber at least 24 h before indentations were performed, in order to minimize the effect of thermal expansion or contraction during the indentation process. The locations for nanoindentation were precisely chosen using scanning probe micrographs taken with the indenter tip. As shown in Fig. 2b, at least 20 valid indentations were performed on the secondary cell wall (S$_2$) structure of each sample in the load-controlled mode, using a three-segment load ramp. The mode consisted of a load application within 5 s, hold time of 30 s, and an unloading time of 5 s in the axial direction of wood fibers. The peak load was 200 μN for all indentations. The 30-s load-holding segment between the loading and unloading segments allowed for the investigation of the visco-elastic properties of the cell wall. Three repeated measurements were conducted on each type of wood sample, respectively.The reduced elastic modulus (E_r) and hardness (H) were calculated from the load-displacement curves

recorded during the experiment (Fig. 2c), according to Oliver and Pharr's (1992) method as follows,

$$H = \frac{P_{max}}{A} \tag{3}$$

where P_{max} is the peak load (N) and A is the projected contact area at the peak load (m^2),

$$E_r = \frac{\sqrt{\pi}}{2\beta} \frac{S}{\sqrt{A}} \tag{4}$$

where E_r is reduced modulus, which accounts for the fact that the elastic deformation occurs in both the sample and the indenter (GPa), S is initial unloading stiffness (GPa), *i.e.*, the slope (dP/dh) of the line tangent to the initial unloading curve in the load-displacement plot, and β is a correction factor correlated to indenter geometry ($\beta = 1.034$ for a Berkovich indenter).
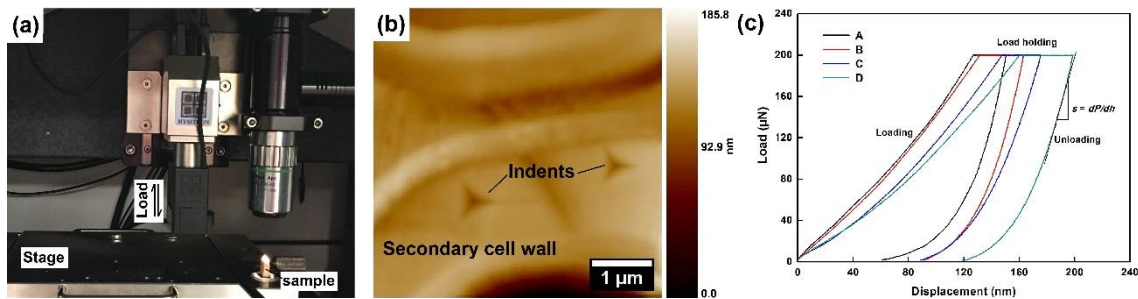

Fig. 2. Nanoindentation set-up: (a) wood sample mounted in Hysitron TriboIndenter, (b) scanning probe microscopy image showing the residual indentation marks on the secondary cell walls, and (c) typical indentation curves of wood samples

Rheological models during nanoindentation

Visco-elastic materials exhibit both elastic and viscous behavior. Linear elastic deformation of materials is described by Hooke's law, which relates the elastic stress, σ, to the elastic strain, ε. The relative change in dimension was calculated according to the following equation,

$$\sigma = E \cdot \varepsilon \tag{5}$$

where E is the elastic modulus in the nanoindentation case (GPa). On the other hand, the viscous component was modeled as a dashpot, as shown in Fig. 3. The relationship between the stress and strain rate can be expressed by Newton's law,

$$\sigma = \eta \cdot \frac{d\varepsilon}{dt} = \eta \cdot \dot{\varepsilon} \tag{6}$$

where the strain rate $\dot{\varepsilon}$ (%) is proportional to the stress and η is the viscosity of a material (GP·s). For creep testing, the stress was held constant ($\sigma = \sigma_0$), and the creep compliance, J (t), was defined as:

$$J(t) = \frac{\varepsilon(t)}{\sigma_0} \tag{7}$$

The load, *P*, contact area, *A*, and indentation depth, *h*, are three important parameters in nanoindentation. The tip used in all of these experiments was a pyramidal indenter (Berkovich tip). According to the method by Schiffmann (2006), the representative stress was given by $\sigma = P/A$, and the representative strain was defined as $d\varepsilon = \cot\delta \cdot dh/h$; thus, the creep compliance was derived as follows,

$$J(t) = \frac{1}{c}\frac{A(t)}{P_0} \qquad c = 2(1 - \upsilon^2) \cdot \tan\delta \tag{8}$$

where υ is the Poisson ratio and δ is the half opening angle of the indenter (70° Berkovich). The load, $P_0 = P(0)$, was obtained directly by the instrument; however, the contact area, $A(t)$, had to be calculated from the area function of the tip (Oliver and Pharr 1992).

Burger's model

For the evaluation of different visco-elastic materials, Maxwell and Kelvin-Voigt models have been developed to predict the deformation of materials (Findley *et al*. 1977). The Maxwell model elements are represented by a purely viscous damper and a purely elastic spring connected in series. The Kevin-Voigt model consists of a purely viscous damper and a purely elastic spring connected in parallel. In this work, the Burger's model, which contains a combination of Maxwell and Kelvin-Voigt model elements, was applied to rationalize the nanoindentation on the wood cell wall (Fig. 3). The relationship between the stress, σ, and the deformation, ε, of the visco-elastic material is given as follows (Findley *et al*. 1977),

$$\sigma + p_1\dot{\sigma} + p_2\ddot{\sigma} = q_1\dot{\varepsilon} + q_2\ddot{\varepsilon} \tag{9}$$

where $\dot{\sigma}$, $\ddot{\sigma}$, $\dot{\varepsilon}$, and $\ddot{\varepsilon}$ are defined as the first and second time derivatives of stress and deformation, respectively, and p_1, p_2, q_1, and q_2 are defined as:

$$p_1 = \frac{\eta_1}{E_1} + \frac{\eta_1}{E_2} + \frac{\eta_2}{E_2} \qquad p_2 = \frac{\eta_1\eta_2}{E_1E_2} \qquad q_1 = \eta_1 \qquad q_2 = \frac{\eta_1\eta_2}{E_2} \tag{10}$$

The parameters E_1 and E_2 are the spring constants (GPa) and η_1 and η_2 are the viscosities (GPa), as described in the Burger's model.

For creep testing, the stress, σ, was held constant, *i.e.*, $\dot{\varepsilon}\ddot{\varepsilon}\dot{\sigma} = \ddot{\sigma} = 0$. Consequently, Eq. (9) can be simplified as follows:

$$\sigma = q_1\dot{\varepsilon} + q_2\ddot{\varepsilon} \tag{11}$$

By applying this equation to Eq. (7), a solution can be written for the form of creep compliance,

$$J(t) = J_0 + J_1 t + J_2\left[1 - exp(-t/\tau_0)\right] \tag{12}$$

where $J_0 = 1/E_1$, $J_1 = 1/\eta_1$, $J_2 = 1/E_2$, and $\tau_0 = \eta_2/E_2$, and τ_0 is the retardation time (s), which describes the retarded elastic deformation of the Kelvin-Voigt model elements in the Burger's model.
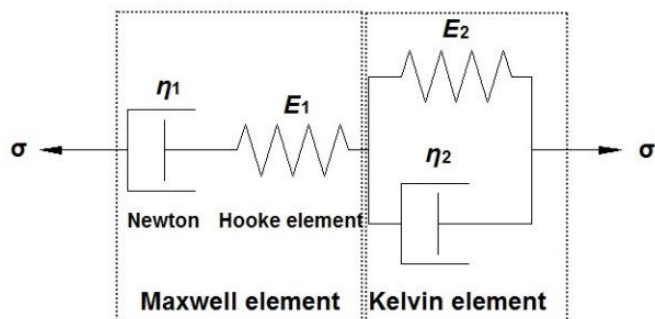
Fig. 3. A spring-dashpot representation of the four-elements of the Burger's model

RESULTS AND DISCUSSION

Main Chemical Components

The relative contents of the main chemical components of the control and treated wood cell walls were determined in order to assess the effectiveness of selective chemical extraction. As shown in Table 1, the solvent extractive content of sample B was 0.29%, *i.e.*, almost no solvent extractives remained in the wood cell wall after the benzene-ethanol treatment. The relative hemicellulose, lignin, and cellulose content of sample C was 1.92%, 25.96%, and 65.75%, respectively. The mass loss of the samples after solvent extraction and alkaline treatment are considered for the yield calculation, and the absolute lignin and cellulose content of sample C declined to 18.95% and 47.9%, similar to that of the control sample. Typically, cellulose chains in wood cell walls have a degree of polymerization (DPs) around 10,000, while hemicelluloses are generally reported to have a degree of polymerization (DP) of less than 200. Therefore, hemicelluloses are more soluble, and it has been shown that large amounts can be removed from the wood cell wall by alkali treatment. Lignin determination also yielded the expected results, as the apparent acid-insoluble residue decreased from 19.06% (sample A) to 1.02% (sample D) after the delignification treatment.

Table 1. Main Chemical Components of Wood Cell Walls

Chemical component Content (%)	Sample A	Sample B	Sample C	Sample D
Solvent extractives	2.29	0.29	0.32	0.42
Hemicelluloses	26.51	26.63	1.92	2.66
Lignin	19.06	19.18	25.96	1.02
Cellulose	48.91	49.49	65.75	87.31

Chemical Structure of the Cell Walls

Infrared spectra of the control wood and the wood treated with benzene-ethanol extraction, alkaline, and delignification are shown in Fig. 4. The overall FTIR spectra of sample A and sample B show that, generally, the spectra remained unchanged after organic solvent extraction, *i.e.*, the solvent extraction had a limited influence on the chemical structure of cellulose, hemicelluloses, and lignin (Oh *et al*. 2005). However, the vibration peaks at 1732 and 1240 cm^{-1} were attributed to the C=O stretching of xylan and disappeared after the alkaline treatment (sample C). Moreover, the intensity of the C-O stretching vibration peak (1045 cm^{-1}) decreased in comparison with the peak of the control wood,

indicating the removal of hemicelluloses by alkalization (Yang *et al*. 2007). As shown in the spectrum of sample D, after the delignification treatment, the bands at 1597, 1507, and 1459 cm^{-1}, corresponding to the aromatic skeletal vibration and other lignin related bands (*e.g*. 1648, 1324 cm^{-1}), disappeared (Jungnikl *et al*. 2008). It is evident that there was little to no remaining lignin in sample D, *i.e.*, the lignin in the wood cell wall had been removed by the $NaClO_2$/acetic acid. During all chemical extractions, slight modifications in the peaks at 1368 and 897 cm^{-1} illustrated that the cellulose was the least changeable wood component, relative to the treatments employed in the present study (Zhang *et al*. 2013).
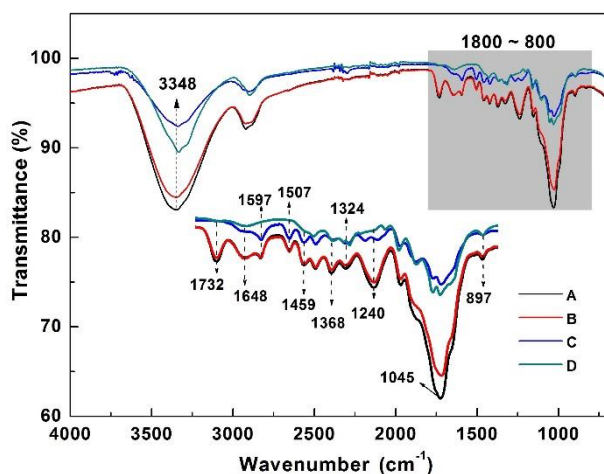

Fig. 4. Fourier transform infrared spectra of wood: sample A (control), sample B (benzene-ethanol extracted), sample C (alkaline treated), and sample D (delignified)

X-Ray Diffraction Results

Figure 5a shows the X-ray diffractograms of the control, benzene-ethanol extracted, alkaline-treated, and delignified wood samples. Generally, the control wood shows the characteristics of cellulose I. The major diffraction planes of cellulose I, namely 101, 002, and 040, are seen at 15.1, 22.5, and 34.6° 2θ angles, respectively (Ouajai and Shanks 2005). The relative degree of crystallinity (C_rI) was calculated from the ratio of the height of the 002 peak (I_{002}) and the height of the minimum (I_{am}), between the 002 and the 101 peaks (Fig. 5b).
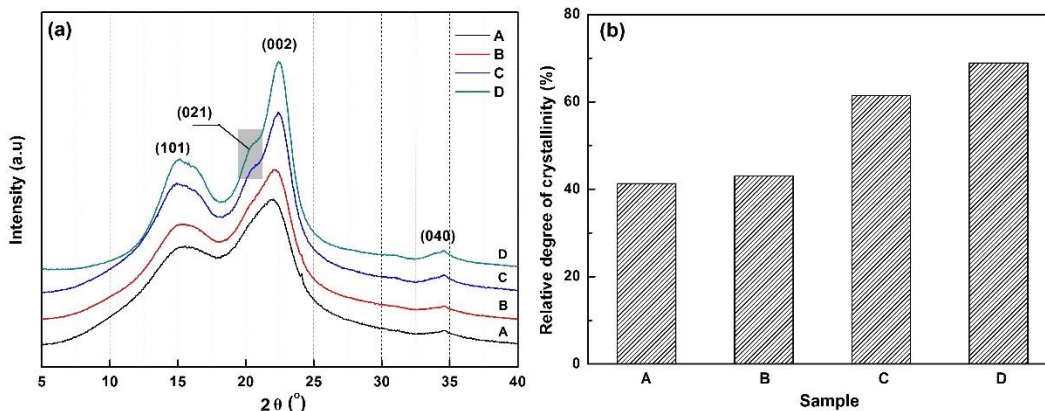

Fig. 5. Crystalline structure: (a) X-ray diffractograms of wood cell walls and the (b) relative degree of crystallinity in the wood samples

Solvent extraction using toluene/ethanol caused almost no change in the cellulose structure and the crystallinity. However, the alkaline treatment and delignification caused a considerable increase in intensity of the 002 plane. The C_rI (%) values of sample C and sample D, after chemical extraction, were 61.4% and 68.9%, respectively, and these values increased to approximately 48.9% and 66.9%, respectively, in comparison to that of the control wood. These results can be explained by the removal of the amorphous hemicelluloses and lignin in the cell walls. A weak 021 peak at 20.4° 2θ angle was observed for sample C and sample D, indicating that there was little crystalline transformation of cellulose II after treatment (Ouajai and Shanks 2005). However, most of the cellulose was present in the form of cellulose I; *i.e.*, the original cellulose crystallite structure was not severely disturbed under the chemical treatment solutions used in this work, which further confirmed the results of the FTIR analysis.

Elastic Modulus and Hardness of Cell Walls

The reduced elastic modulus (E_r) and hardness (H) in the longitudinal direction of the control and treated wood cell walls are shown in Fig. 6. It can be inferred from these two figures that the chemical extraction negatively affected both the elastic modulus and the hardness of the cell walls. The mean values of E_r and H of wood cell walls showed only a slight decrease after solvent extraction, illustrating that organic extractives contributed minimally to the elastic modulus and hardness of wood cell walls. However, in comparison to the control wood cell wall, the absolute reduction (subtracting the reduction attributed to the completed chemical treatment) in the modulus and hardness of sample C's cell wall were 11.7% and 14.8%, respectively. Consequently, the modulus and hardness of the cell wall in sample D decreased by 28.4% and 30.4%, respectively.
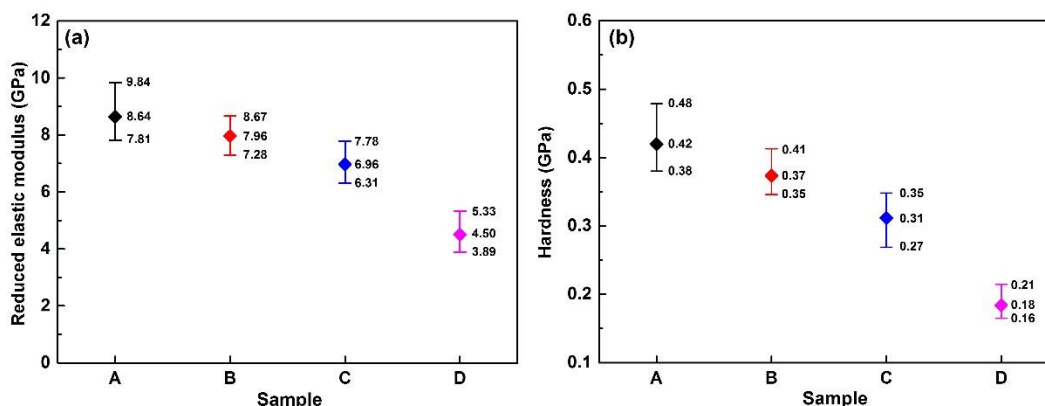

Fig. 6. Nanoindentation measurements of the (a) reduced elastic modulus and (b) hardness of: sample A (control), sample B (benzene-ethanol-extracted), sample C (alkaline-treated), and sample D (delignified)

It can be concluded that the proportions of the main chemical components (cellulose, hemicelluloses, and lignin) in the cell wall have a large effect on the mechanics of wood cell wall (Salmén and Burgert 2009; Wagner *et al.* 2015). Cellulose chains are bonded together through hydrogen bonds, forming a polymer with a hierarchical structure that contributes to the stability, stiffness, and strength of the cell wall. Hemicelluloses, although non-aggregate forming, also contribute to the mechanical properties of the material by bonding to both cellulose and lignin. Lastly, lignin is polymerized to form a complex amorphous network enclosing both cellulose and hemicelluloses during cell-wall

biosynthesis. The lignin network, therefore, contributes to the stiffness of the cell walls (Gindl *et al.* 2002).

Creep Behavior of Cell Walls

Burger's model ideally expresses the stress-strain-time behavior of a material when the material is subjected to a constant stress over time plus an initial strain. Therefore, the visco-elastic properties of wood cell walls were investigated by fitting the indentation depth-time curves to the Burger's model. The experimental creep compliance data for the wood cell walls with different chemical treatments, together with the Burger's model, predicted creep compliance (red line), as shown in Fig. 7. The R^2 correlation coefficient was over 0.99 for all indentations; therefore, the Burger's model was appropriate for predicting the cell walls' visco-elastic behavior. According to Eq. (12) and the fitting parameters, the initial creep compliance, $J(0) = J_0$, at the onset of load holding of the cell walls in sample A, sample B, sample C, and sample D were 0.477 GPa, 0.556 GPa, 0.619 GPa, and 0.874 GPa, respectively. At the end of the load-holding period, the creep compliance, $J(30)$, increased by 38.7%, 41.8%, 50.3%, and 60.4% for sample A, sample B, sample C, and sample D, respectively, meaning that the fiber cell walls deformed more under the constant load after chemical extraction, especially with the alkaline and delignification treatments. The degradation of hemicelluloses and lignin in the cell walls might also weaken the structural continuity and reduced the resistance of the wood cell walls to creep (Zhang *et al*. 2013).
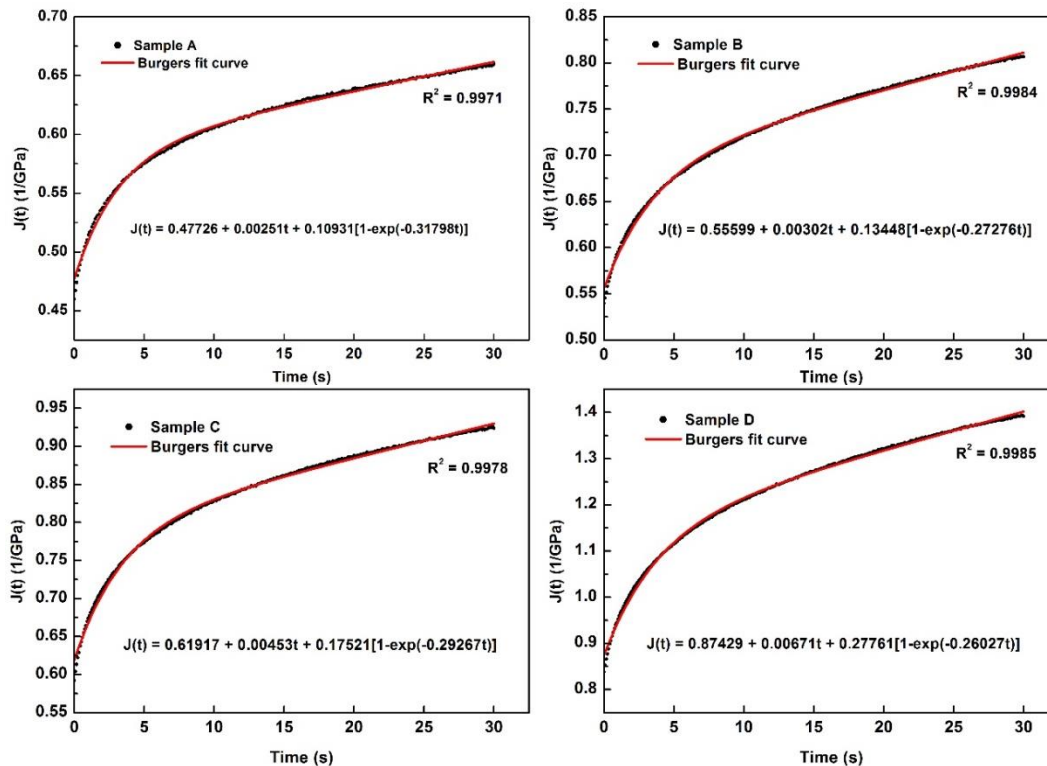

Fig. 7. Representative fit curve of the Burger's model to the holding portion of an indentation curve. All of the best-fit curves had R^2 correlation coefficients over 0.99

The benefit of the four-parameter Burger's model is that the fitting parameters can be interpreted physically as an instantaneous elastic deformation, followed by a visco-

elastic deformation and viscous deformations (Fig. 3). To gain insight into the mechanical function of chemical components of the cell wall, the parameters in the Burger's model include the modulus of elasticity (E_1), modulus of visco-elasticity (E_2), coefficients of viscosity (η_1), and visco-elasticity (η_2), all of which were calculated based on Burger's fit curves and Eq. (12). The effects of the chemical extraction on the visco-elastic behavior, in terms of the fitting parameters, are listed in Table 2. As expected, minor decreases in those four parameters was found, correlating with the removal of solvent extractives. In contrast, a clear decrease was observed after the alkaline treatment. Based on subtracting the reduction ascribed to the completed solvent extraction, the E_1, E_2, η_1, and η_2 of sample C decreased by 8.8%, 18.9%, 27.7%, and 28.4%, respectively, in comparison to that of the control wood cell wall. Interestingly, the reductions of both the η_1 and η_2 were higher than those of the E_1 and E_2 after the removal of hemicelluloses, respectively, *i.e.*, the hemicelluloses showed a greater influence on the viscosity of the cell wall than the elasticity. In fact, hemicelluloses are thought to act as a viscous matrix, in which the fibrils are embedded, providing a mechanically favorable "stick-slip" mechanism when the fiber is loaded beyond elastic deformation (Keckes *et al.* 2003; Konnerth *et al.* 2010). Thus, the degradation of hemicelluloses, especially xylan, may result in a weakening of the flexible connections of the polymers in the cell wall. Furthermore, decreased moisture absorption in the cell wall, because of a reduction in the hydrophilic groups, may be another negative influential factor for the viscosity (Meng *et al.* 2015). The E_1, E_2, η_1, and η_2 of sample D decreased by 22.5%, 23.0%, 17.8%, and 19.7%, respectively, in comparison with the control wood cell wall, after decreases ascribed to the completed solvent and alkaline extraction were subtracted. Apparently, the elasticity of cell-wall is prone to being affected by the lignin content, which is in agreement with the findings of Gindl *et al.* (2002), reporting that lignin fills the spaces between cellulose and hemicellulose strands, and plays an important role in the overall stiffness of the cell wall matrix. Finally, the residual E_1, E_2, η_1, and η_2 occupied 54.6%, 39.5%, 37.4%, and 48.1%, respectively, in comparison with the control wood cell wall, which confirmed that cellulose dominates the mechanical properties of wood cell wall.

Table 2. Elastic and Viscosity Coefficients from the Burgers Fit Curves: Spring Constant (E_1), Spring Constant (E_2), Viscosity (η_1), and Visco-elasticity (η_2)

Coefficients	Sample A	Sample B	Sample C	Sample D
E_1	2.09	1.79	1.62	1.14
E_2	9.15	7.44	5.71	3.60
η_1	398.41	331.13	220.75	149.76
η_2	28.77	27.26	19.50	13.84

CONCLUSIONS

1. Nanoindentation was performed on wood cell walls to investigate the particular contributions of principal chemical components to the mechanical properties of cell walls.

2. Wood extractives, hemicelluloses, and lignin were removed from the wood cell wall gradually and effectively, which was beneficial for evaluating the mechanical function of each cell wall component, separately.

3. Wood extractives showed a limited influence on the mechanics of cell wall, whereas the removal of hemicelluloses and lignin resulted in a considerable decrease in the cell walls' elastic modulus and hardness, and led to an obvious increase in the creep compliance.

4. Based on Burger's model, cellulose dominated the mechanical properties of wood cell wall, while hemicelluloses make a greater contribution to the viscosity of cell wall and lignin contributes primarily to the elasticity of cell wall.

ACKNOWLEDGMENTS

REFERENCES CITED

Abraham, E., Deepa, B., Pothan, L. A., Jacob, M., Thomas, S., Cvelbar, U., and Anandjiwala, R. (2011). "Extraction of nanocellulose fibrils from lignocellulosic fibres: A novel approach," *Carbohydr. Polym.* 86(4), 1468-1475. DOI: 10.1016/j.carbpol.2011.06.034

Askanian, H., Verney, V., Commereuc, S., Guyonnet, R., and Massardier, V. (2015). "Wood polypropylene composites prepared by thermally modified fibers at two extrusion speeds: Mechanical and viscoelastic properties," *Holzforschung* 69(3), 313-319. DOI: 10.1515/hf-2014-0031

Browning, B. L. (1967). *Method of Wood Chemistry*, Vol. II., Interscience/Wiley, New York, USA. DOI: 10.1002/pol.1968.160061112

Findley, W. N., Lai, J. S., Onaran, K., and Christensen, R. M. (1977). "Creep and relaxation of nonlinear viscoelastic materials with an introduction to linear viscoelasticity," *J. Appl. Mech.* 44(2), 364. DOI: 10.1115/1.3424077

GB/T 2677.6 (1994). "Fibrous raw material-Determination of solvent extractives," China State Administration of Quality Supervision Inspection and Quarantine Chinese Standard, China.

GB/T 2667.8 (1994). "Fibrous raw material-Determination of acid-insoluble lignin," China State Administration of Quality Supervision Inspection and Quarantine Chinese Standard, China.

Gindl, W., Gupta, H. S., and Grunwald, C. (2002). "Lignification of spruce tracheids secondary cell wall related to longitudinal hardness and modulus of elasticity using nano-indentation," *Can. J. Bot.* 80(10), 1029-1033. DOI: 10.1139/b02-091

bioresources.com

Jungnikl, K., Paris, O., Fratzl, P., and Burgert, I. (2008). "The implication of chemical extraction treatments on the cell wall nanostructure of softwood," *Cellulose* 15(3), 407-418. DOI: 10.1007/s10570-007-9181-5

Kataoka, Y., and Kondo, T. (1998). "FT-IR microscopic analysis of changing cellulose crystalline structure during wood cell wall formation," *Macromol.* 31(3), 760-764. DOI: 10.1021/ma970768c

Keckes, J., Burgert, I., Frühmann, K., Müller, M., Kölln, K., Hamilton, M., Burghammer, M., Roth, S. V., Stanzl-Tschegg, S., and Fratzl, P. (2003). "Cell-wall recovery after irreversible deformation of wood," *Nat. Mater.* 2(12), 810-814. DOI: 10.1038/nmat1019

Konnerth, J., Eiser, M., Jäger, A., Bader, T. K., Hofstetter, K., Follrich, J., Ters, T., Hansmann, C., and Wimmer, R. (2010). "Macro- and micro-mechanical properties of red oak wood (*Quercus rubra* L.) treated with hemicellulases," *Holzforschung* 64(4), 447-453. DOI: 10.1515/hf.2010.056

Li, Y., Yin, L., Huang, C., Meng, Y., Fu, F., Wang, S., and Wu, Q. (2015). "Quasi-static and dynamic nanoindentation to determine the influence of thermal treatment on the mechanical properties of bamboo cell walls," *Holzforschung* 69(7), 909-914. DOI: 10.1515/hf-2014-0112

Meng, Y., Wang, S., Cai, Z., Young, T. M., Du, G., and Li, Y. (2013). "A novel sample preparation method to avoid influence of embedding medium during nano-indentation," *Appl. Phys. A* 110(2), 361-369. DOI: 10.1007/s00339-012-7123-z

Meng, Y., Xia, Y., Young, T. M., Cai, Z., and Wang, S. (2015). "Viscoelasticity of wood cell walls with different moisture content as measured by nanoindentation," *RSC Adv.* 5(59), 47538-47547. DOI: 10.1039/C5RA05822H

Nelson, R. (1961). "The use of holocellulose to study cellulose supermolecular structure," *J. Polym. Sci.* 51(155), 27-58. DOI: 10.1002/pol.1961.1205115504

Nishino, T., Matsuda, I., and Hirao, K. (2004). "All-cellulose composite," *Macromol.* 37(20), 7683-7687. DOI: 10.1021/ma049300h

Oh, S. Y., Yoo, D. I., Shin, Y., Kim, H. C., Kim, H. Y., Chung, Y. S., Park, W. H., and Youk, J. H. (2005). "Crystalline structure analysis of cellulose treated with sodium hydroxide and carbon dioxide by means of X-ray diffraction and FTIR spectroscopy," *Carbohydr. Res.* 340(15), 2376-2391. DOI:10.1016/j.carres.2005.08.007

Oliver, W. C., and Pharr, G. M. (1992). "An improved technique for determining hardness and elastic modulus using load and displacement sensing indentation experiments," *J. Mater. Res.* 7(06), 1564-1583. DOI: 10.1557/JMR.1992.1564

Ouajai, S., and Shanks, R. A. (2005). "Component, structure and thermal degradation of hemp cellulose after chemical treatments," *Polym. Degrad. Stab.* 89(2), 327-335. DOI:10.1016/j.polymdegradstab.2005.01.016

Placet, V., Passard, J., and Perré, P. (2007). "Viscoelastic properties of green wood across the grain measured by harmonic tests in the range 0-95 °C: Hardwood vs. softwood and normal wood vs. reaction wood," *Holzforschung* 61(5), 548-557. DOI: 10.1515/HF.2007.093

Salmén, L., and Burgert, I. (2009). "Cell wall features with regard to mechanical performance. A review," *Holzforschung* 63(2), 121-129. DOI: 10.1515/HF.2009.011

Schiffmann, K. I. (2006). "Nanoindentation creep and stress relaxation tests of polycarbonate: Analysis of viscoelastic properties by different rheological models," *Int. J. Mater. Res.* 97(9), 1199-1211. DOI: 10.3139/146.101357

Segal, L., Creely, J. J., Martin, A. E., and Conrad, C. M. (1959). "An empirical method for estimating the degree of crystallinity of native cellulose using the X-ray diffractometer," *Textile. Res. J.* 29(10), 786-794. DOI: 10.1177/004051755902901003

Wagner, L., Bader, T. K., Ters, T., Fackler, K., Borst, K. D. (2015). "A combined view on composition, molecular structure, and micromechanics of fungal degraded softwood," *Holzforschung* 69(4), 471-482. DOI: 10.1515/hf-2014-0023

Wang, X., Deng, Y., Wang, S., Liao, C., Meng, Y., and Pham, T. (2013). "Nanoscale characterization of reed stalk fiber cell walls," *BioResources* 8(2), 1986-1996. DOI: 10.15376/biores.8.2.1986-1996

Wang, X., Deng, Y., Wang, S., Chen, M., Meng, Y., Pham, T., and Yang, Y. (2014). "Evaluation of the effects of compression combined with heat treatment by nanoindentation (NI) of poplar cell walls," *Holzforschung* 68(2), 167-173. DOI: 10.1515/hf-2013-0084

Wimmer, R., Lucas, B. N., Oliver, W. C., and Tsui, T. Y. (1997). "Longitudinal hardness and Young's modulus of spruce tracheid secondary walls using nanoindentation technique," *Wood Sci. Technol.* 31(2), 131-141. DOI: 10.1007/BF00705928

Wise, L. E., Murphy, M., and D'Addieco, A. A. (1946). "Chlorite holocellulose, its fractionation and bearing on summative wood analysis and on studies on the hemicelluloses," *Paper Trade J.* 122(2), 35-43.

Yang, H., Yan, R., Chen, H., Lee, D. H., and Zheng, C. (2007). "Characteristics of hemicelluloses, cellulose and lignin pyrolysis," *Fuel* 86(12-13), 1781-1788. DOI: 10.1016/j.fuel.2006.12.013

Yu, Y., Tian, G., Wang, H., Fei, B., and Wang, G. (2011). "Mechanical characterization of single bamboo fibers with nanoindentation and microtensile technique," *Holzforschung* 65(1), 113-119. DOI: 10.1515/hf.2011.009

Zelinka, S. L., Lambrecht, M. J., Glass, S. V., Wiedenhoeft, A. C., and Yelle, D. J. (2012). "Examination of water phase transitions in Loblolly pine and cell wall components by differential scanning calorimetry," *Thermochim. Acta* 533, 39-45. DOI: 10.1016/j.tca.2012.01.015

Zhang, S. Y., Wang, C. G., Fei, B. H., Yu, Y., Cheng, H. T., and Tian, G. L. (2013). "Mechanical function of lignin and hemicelluloses in wood cell wall revealed with microtension of single wood fiber," *BioResources* 8(2), 2376-2385. DOI: 10.15376/biores.8.2.2376-2385